Short Isoforms of the Cold Receptor TRPM8 Inhibit Channel Gating by Mimicking Heat Action Rather than Chemical Inhibitors

José A Fernández, Roman Skryma, Gabriel Bidaux, Karl L Magleby, C. Norman Norman Scholfield, J. Graham Graham Mcgeown, Natalia Prevarskaya, Alexander V Zholos

THE JOURNAL OF BIOLOGICAL CHEMISTRY VOL. 287, NO. 5, pp. 2963–2970, January 27, 2012

Short Isoforms of the Cold Receptor TRPM8 Inhibit Channel Gating by Mimicking Heat Action Rather than Chemical Inhibitors*[S]

Received for publication, June 16, 2011, and in revised form, November 24, 2011 Published, JBC Papers in Press, November 28, 2011, DOI 10.1074/jbc.M111.272823

José A. Fernández[‡1], Roman Skryma[§], Gabriel Bidaux[§], Karl L. Magleby[¶], C. Norman Scholfield[**], J. Graham McGeown[‡], Natalia Prevarskaya[§], and Alexander V. Zholos[‡2]

From the [‡]Center for Vision and Vascular Science, Queen's University Belfast, BT12 6BA Belfast, United Kingdom, the [§]Laboratory of Cell Physiology, INSERM U800, Lille University of Science and Technology, 59655 Villeneuve d'Ascq, France, the [¶]Department of Physiology and Biophysics, University of Miami Miller School of Medicine, Miami, Florida 33101, and the [**]Faculty of Pharmaceutical Sciences, Naresuan University, Phitsanulok 65000, Thailand

Background: Mechanistic understanding of complex regulation of sensory transient receptor potential (TRP) channels can be facilitated by quantitative single-channel analysis.
Results: Inhibition of the cold receptor TRPM8 by short isoforms, heat, and chemical blockers shows different sets of common single-channel kinetic features.
Conclusion: Short channel isoforms mimic heat action rather than chemical inhibitors.
Significance: This is the first indication that different classes of TRPM8 inhibition may exist.

Transient receptor potential (TRP) channels couple various environmental factors to changes in membrane potential, calcium influx, and cell signaling. They also integrate multiple stimuli through their typically polymodal activation. Thus, although the TRPM8 channel has been extensively investigated as the major neuronal cold sensor, it is also regulated by various chemicals, as well as by several short channel isoforms. Mechanistic understanding of such complex regulation is facilitated by quantitative single-channel analysis. We have recently proposed a single-channel mechanism of TRPM8 regulation by voltage and temperature. Using this gating mechanism, we now investigate TRPM8 inhibition in cell-attached patches using HEK293 cells expressing TRPM8 alone or coexpressed with its short sM8-6 isoform. This is compared with inhibition by the chemicals *N*-(4-*tert*-butylphenyl)-4-(3-chloropyridin-2-yl)piperazine-1-carboxamide (BCTC) and clotrimazole or by elevated temperature. We found that within the seven-state single-channel gating mechanism, inhibition of TRPM8 by short sM8-6 isoforms closely resembles inhibition by increased temperature. In contrast, inhibition by BCTC and that by clotrimazole share a different set of common features.

Temperature-sensitive transient receptor potential (TRP)[3] channels are activated by various chemical compounds that mimic the sensation of heat or cold. For example, TRPM8 is activated by the "cooling" compound menthol (1–3). It has also been recently reported that the effects of different modulators on TRPM8 gating are bidirectional (4). The regulatory effects of several antagonists on TRPM8 whole-cell currents have already been studied (4–9). Two compounds, *N*-(4-*tert*-butylphenyl)-4-(3-chloropyridin-2-yl)piperazine-1-carboxamide (BCTC) and clotrimazole, have been identified as potent TRPM8 inhibitors. In this study, the effects of these chemical antagonists are compared with physiological channel inhibition by temperature and with that seen in the presence of one of the shorter splice variants, sM8-6, of the full-length channel (10).

Alternative mRNA splicing is an important regulatory process that contributes to biological complexity and diversity by altering the primary structure of proteins expressed from a single gene (11). Function may be altered through production of nonfunctional isoforms or alterations in domains necessary for channel opening or subcellular localization. Most TRP channels can be expressed in two or more shorter splice variants that may exhibit different expression profiles in different tissues compared with full-length forms (12). Several examples of altered regulation, function, and ion selectivity have been described, as well as loss of channel function (12). For example, we recently found that the full-length TRPC4α channel and its shorter TRPC4β isoform differ in their regulation by phosphatidylinositol 4,5-bisphosphate (13). A dominant-negative loss-of-function effect is another common feature attributed to short TRP splice variants (12). The underlying mechanism is not clear, however, as it may involve reduced channel expression, diminished channel function, or a combination of these two. Quantitative descriptions of the effects of such isoforms in terms of a single-channel gating mechanism would help resolve these questions.

TRPM8 splice variants with an altered N terminus have been cloned from lung epithelia and cancerous prostate (11). Recent

* This work was supported by the European Social Fund (to A. V. Z., J. G. M., C. N. S., and J. A. F.) and by National Institutes of Health Grant AR32805 (to K. L. M.).
[S] This article contains supplemental Figs. S1–S4 and Tables S1–S7.
[1] To whom correspondence may be addressed. E-mail: jfernandezgonzalez01@qub.ac.uk.
[2] To whom correspondence may be addressed: Dept. of Biophysics, Institute of Biology, Taras Shevchenko National University of Kyiv, 01601 Kyiv, Ukraine. Tel.: 380 44 521 3325; Fax: 380 44 521 3598; E-mail: a.zholos@qub.ac.uk.
[3] The abbreviations used are: TRP, transient receptor potential; BCTC, *N*-(4-*tert*-butylphenyl)-4-(3-chloropyridin-2-yl)piperazine-1-carboxamide; P_o, channel open probability.

evidence suggests that some of these isoforms may serve as dominant-negative regulators of full-length TRPM8 (11). In support of this suggestion, our accompanying article (10) describes the short sM8-18 and sM8-6 isoforms of TRPM8. These are similar to a previously described N terminus-derived short TRPC2 isoform lacking all transmembrane domains and therefore the pore, which is capable of interacting with the full-length channel to inhibit Ca^{2+} entry via TRPC2 (14). The purpose of this study was to determine the single-channel gating mechanisms underlying the inhibition of TRPM8 channels by coexpression of the short isoform sM8-6 (10) and to compare this to inhibition by elevated temperature and chemical modulators. This should provide insight into the mechanism of action underlying sM8-6 inhibition. We first show that our recent single-channel model of TRPM8 regulation by voltage and temperature (15) provides a suitable framework to interpret single-channel activity in the presence of the different inhibitors: sM8-6, BCTC, and clotrimazole. A comparison of the parameters describing channel gating then allowed us to identify similarities and differences in underlying gating mechanisms. Inhibition of TRPM8 by sM8-6 was most similar to inhibition by increasing temperature. In contrast, inhibition by BCTC and clotrimazole had many features in common but differed from that by sM8-6 and increased temperature, suggesting differences in the underlying mechanism. The mechanistic similarities between the actions of increasing temperature and sM8-6 isoforms provide a possible explanation for the pervasive physiological presence of TRPM8 channels in tissues where there is little temperature variation, as short isoforms may exploit similar molecular mechanisms as temperature to alter channel activity. Short TRPM8 isoforms appear to act on the channel by mimicking the effects of increased temperature, presumably by changing the conformation of one or more temperature-sensitive regions in the full-length channel.

EXPERIMENTAL PROCEDURES

Cell Culture—TRPM8 expression was induced by tetracycline in HEK293 cells maintained in DMEM (Invitrogen) supplemented with 10% FBS (Invitrogen) and 1% kanamycin (16). sM8-6 proteins encoded by the sM8β splice variant were expressed as described (10).

Electrophysiology and Solutions—Membrane currents were recorded either at room temperature (20–23 °C) or at 30 °C in the cell-attached configuration using an Axopatch 200B amplifier (Molecular Devices, Union City, CA). Data are from recordings at room temperature unless indicated otherwise. Currents through single TRPM8 channels were recorded and analyzed as described (15). The bath solution initially contained 150 mM NaCl, 1 mM $MgCl_2$, 5 mM glucose, and 10 mM HEPES, pH 7.3 (adjusted with NaOH). Because TRPM8 is weakly voltage-dependent, being activated by membrane depolarization, to quickly record a sufficiently large number of single-channel events, cell-attached patches were held at 100 or 120 mV positive to the resting potential, which was brought close to 0 mV by equimolar substitution of KCl for NaCl in the bath solution. Rate constants for sM8-6 isoforms recorded at +120 mV were corrected to +100 mV using partial charge estimates from a previous study (15) for comparisons of shifts in rate constants with the other inhibitors at +100 mV. The same findings were obtained for corrected and uncorrected sM8-6 data. The pipettes were filled with the same solution used initially for the bath. Pharmacological inhibition was achieved by adding BCTC (stock solution of 10 mM in Me_2SO; BIOMOL International) or clotrimazole (stock solution of 10 mM in ethanol; Sigma-Aldrich) to the bath solution.

Fitting Models to Experimental Data—The single-channel analysis methods used to measure interval durations with the 50% threshold crossing method, to estimate rate constants, and to evaluate kinetic models have been extensively described (17–27). A seven-state kinetic model (see Fig. 4) was fitted to the two-dimensional dwell-time distributions using maximum likelihood methods (15, 26, 27) to determine the most likely rate constants for transitions among states, as well as the equilibrium occupancies of the states. Whereas each modulator gave large, relatively characteristic visual shifts in the dwell-time distributions for data from different single channels, the estimates of the rate constants for the seven-state model could show considerable variability among different single-channel patches, as is often the case for single-channel data (15). Consequently, even though the distributions and gating were well described by the model and rate constants for any given single-channel data, the standard errors for the means of combined data were large, so few of the changes in the estimated rate constants were significant.

Therefore, to explore similarities and differences in the mechanisms of the various modulators, we examined whether the various modulators acted in the same or a different manner on each of the rate constants using the equivalent of a binomial sign test. The rational for the test is that modulators that act through similar mechanisms might be expected to have similar effects on the various rate constants. To assess the findings, we calculated the probability of the observed direction of changes in rate constants for two compared modulators occurring by chance alone as follows. For each of the 12 rate constants, two random numbers between 0 and 1 were drawn. If the two random numbers for a given rate constant were both $\geq$0.5 or both $<$0.5, then the rate constants were considered changed in the same direction by both modulators. For a given trial, the number of rate constants changed in the same direction by both modulators for the 12 rate constants was tabulated and then binned into an array with addresses from 12 to 0. This process was repeated 10^7 times. Dividing each of the bins by 10^7 then gave the probability of observing 12, 11, 10, 9, and down to 0 of the rate constants changed in the same direction for the two compared modulators by chance alone. The probabilities from simulation were the same as those obtained from the binomial distribution with $n = 12$ and $p = 0.5$ to obtain 0.000244, 0.00293, 0.0161, 0.0537, 0.121, 0.193, 0.226, 0.193, 0.0121, 0.0537, 0.0161, 0.00293, and 0.000244. Cumulative probabilities were then tabulated such that the probabilities of observing 12, 11 or more, 10 or more, 9 or more, 8 or more, 7 or more, and 6 or more of the 12 rate constants changed in the same direction by chance alone were 0.000244, 0.00317, 0.0193, 0.0730, 0.194, 0.387, and 0.613. It is these cumulative probabilities that are used in the study. They can be calculated using Equation 1,

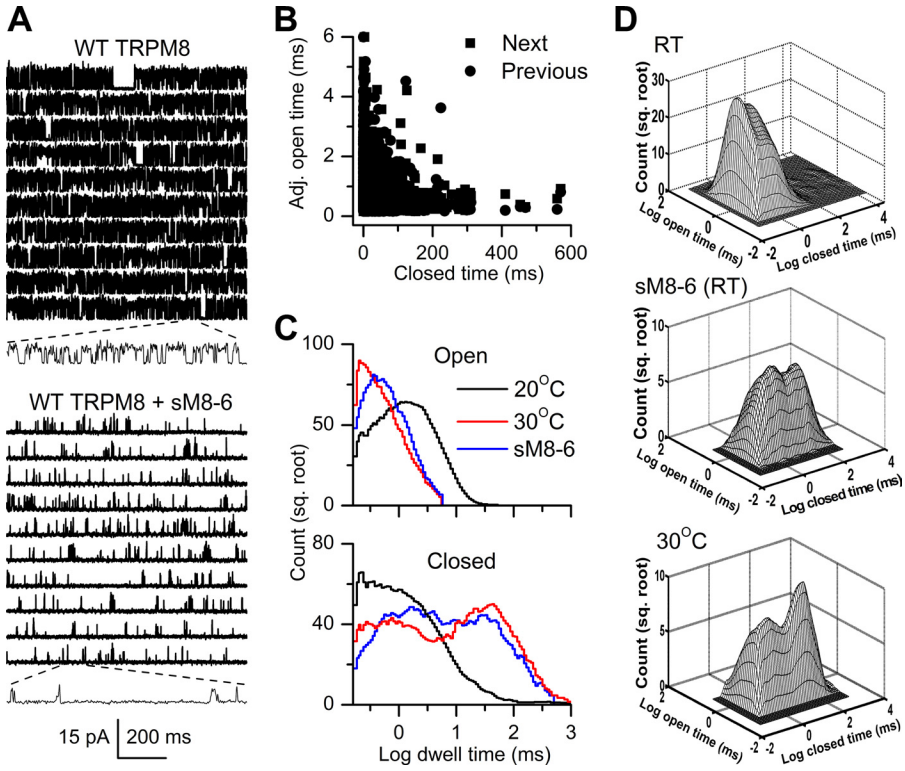

FIGURE 1. **Effects of sM8-6 isoforms on activity of full-length (WT) TRPM8.** *A*, representative single-channel traces recorded in the cell-attached configuration at room temperature in HEK293 cells expressing WT TRPM8 (*upper panel*) or both WT TRPM8 and sM8-6 proteins (*lower panel*). Note the short current segments shown on a 10-fold expanded time scale for both examples. Upward currents indicate channel opening. *B*, inverse correlation between adjacent (*Adj.*) open and closed interval durations for TRPM8 expressed with sM8-6 isoforms. Data points represent 4523 pairs of closed and adjacent open intervals (with previous and next shown by different symbols) measured from the patch illustrated in *A*. Compare with Fig. 4*A* in Ref. 15 for similar correlations present in WT TRPM8. *C*, open (*upper panel*) and closed (*lower panel*) one-dimensional dwell-time distributions as histograms (25 bins per decade) plotted for WT TRPM8 at 20 °C (*black lines*; from Ref. 15), coexpressed with sM8-6 isoforms (*blue lines*), and at 30 °C (*red lines*; from Ref. 15). These histograms have been normalized to the same number of events to facilitate comparisons. A moving bin average of three bins has been applied to the histograms to smooth stochastic variation. *sq.*, square. *D*, two-dimensional dwell-time distributions for representative currents from WT TRPM8 currents at room temperature (*RT*) (*upper panel*; from Ref. 15), TRPM8 with sM8-6 isoforms at room temperature (*middle panel*), and TRPM8 at 30 °C (*lower panel*; from Ref. 15).

$$P_B = \sum_{i=X}^{N} \binom{N}{i} \times P^i \times (1-P)^{N-i} \qquad \text{(Eq. 1)}$$

where P_B is the cumulative probability (which is the sum of the binomial distribution probabilities) for getting X or more of N rate constants changed in the same direction by chance alone ($p = 0.5$). The binomial of N and i is shown in Equation 2,

$$\binom{N}{i} = \frac{N!}{i! \times (N-i)!} \qquad \text{(Eq. 2)}$$

where $N! = 1 \times 2 \ldots \times N$. The cumulative probabilities can also be calculated using GraphPad Software QuickCalcs by selecting sign test and then binomial and sign test.

Statistics—Average data are expressed as means ± S.E., where n equals the number of patches or cells. Where appropriate, Mann-Whitney and nonparametric repeated measures analysis of variance tests were conducted using InStat 3.05 (GraphPad Software).

RESULTS

Coexpression with sM8-6 Isoforms Decreases Open Probability of WT TRPM8 Channels Mainly by Shifting Closed Intervals toward Longer Durations—Fig. 1*A* shows representative single-channel currents recorded at room temperature from a WT TRPM8 channel (*upper panel*) and from a TRPM8 channel coexpressed with sM8-6 isoforms (*lower panel*). A pronounced decrease in channel open probability (P_o) was induced by the sM8-6 isoforms (10), which increased channel closed times from 1.67 ± 0.27 ms ($n = 6$) to 22.7 ± 5.8 ms ($n = 5$; $p = 0.0043$). There was a parallel but much smaller decrease in mean open times, from 1.83 ± 0.13 ms ($n = 6$) to 0.85 ± 0.11 ms ($n = 5$; $p = 0.0043$). Thus, sM8-6 isoforms inhibit TRPM8 activity mainly by decreasing the frequency of channel openings rather than the duration. A similar decrease in closed times with smaller changes in open times is also seen with increased temperature and at negative membrane potentials (15). An inverse correlation between adjacent open and closed interval durations described previously for WT TRPM8 channels (15) was retained in the presence of sM8-6 isoforms (Fig. 1*B*), suggesting that the two or more independent connections between open and closed states in WT TRPM8 channels are retained in the presence of sM8-6 isoforms.

The shifts in the closed interval durations observed in the single-channel records were also revealed in the one- and two-dimensional dwell-time distributions. Coexpression with sM8-6 isoforms produced a shift from briefer toward longer closed intervals, with less of a shift from longer to briefer open intervals. This can be seen both for the one-dimensional open and closed dwell-time distributions (Fig. 1*C*, *black lines* for WT

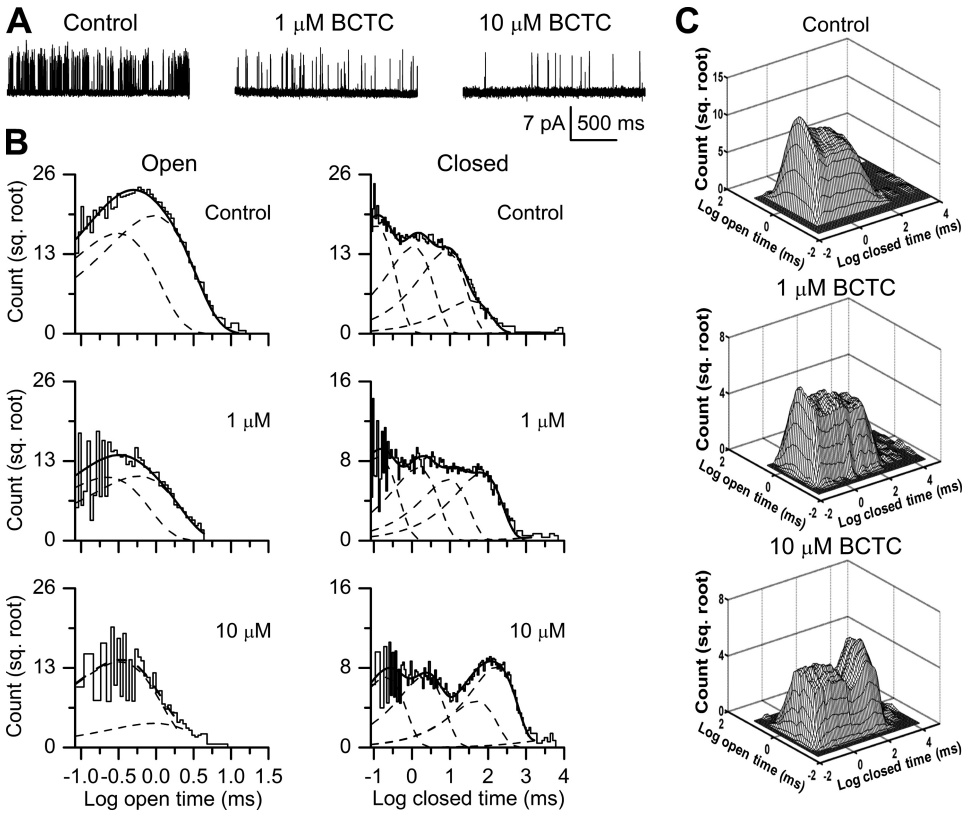

FIGURE 2. **Effects of BCTC on single-channel WT TRPM8 currents.** *A*, representative traces of single-channel activity in 0 (control), 1, and 10 μM BCTC as indicated recorded from the same patch at room temperature. *B*, open and closed one-dimensional dwell-time histograms for the same conditions. The histograms have been fitted (*continuous lines*) by the sum of two open and five closed exponential components (*dashed lines*). *sq.*, square. *C*, representative two-dimensional dwell-time distributions.

TRPM8 alone and *blue lines* for coexpression of sM8-6 isoforms) and the two-dimensional dwell-time distributions of adjacent open and closed interval durations (Fig. 1*D*, *upper* and *middle panels*). In both cases, the effects of sM8-6 at room temperature were similar to those of increased temperature (30 °C) on WT TRPM8 alone (Fig. 1, *C*, *red lines*, and *D*, *lower panel*).

The shifts in the one-dimensional distributions were quantified by fitting with sums of exponential components. The histograms of dwell times with coexpressed sM8-6 were typically described by two significant open and five significant closed components (supplemental Fig. S1, *dashed lines*, representing analysis of data in Fig. 1*A*, *lower panel*), similar to full-length TRPM8 expressed alone (15). The areas and time constants of the exponential components for TRPM8 gating in the absence and presence of coexpression with sM8-6 are provided in supplemental Table S1. sM8-6 significantly reduced the time constants of both open components, increased the area of the brief open component, and decreased the area of the long open component, indicating an overall shift from longer to briefer openings. In addition, the area of the briefest closed component (EC1) decreased, the time constant of the next to longest closed component (EC4) increased, and the time constant of the longest closed component (EC5) greatly decreased. The area of the two longest closed components (EC4 and EC5) increased by 11- and 286-fold, respectively, moving 37% of the area into the longer closed components compared with only 2.5% for WT TRPM8. The changes described above suggest that the sM8-6 isoforms modulate the activity of WT TRPM8 channels by shifting areas and time constants of the underlying exponential components describing the dwell-time distributions without affecting the major kinetic structure of channel gating.

BCTC and Clotrimazole Inhibit TRPM8 Activity Mainly by Increasing Closed Interval Durations—Fig. 2*A* shows TRPM8 single-channel currents through a representative patch recorded at room temperature before and after application of BCTC. A dose-dependent decrease in channel activity is readily apparent with increasing BCTC concentration. P_o decreased from 0.13 ± 0.03 to 0.04 ± 0.01 with 1 μM BCTC and to 0.03 ± 0.03 with 10 μM BCTC ($n = 10$; $p = 0.0036$). As with sM8-6 isoforms, these P_o reductions resulted mainly from increases in mean closed times, *i.e.* the mean closed time significantly increased from 7.5 ± 1.6 ms in the control to 28 ± 10 ms with 1 μM BCTC and to 118 ± 77 ms with 10 μM BCTC ($n = 10$; $p = 0.0036$). Although also significant, the decrease in mean open times was much smaller in comparison (0.69 ± 0.04, 0.50 ± 0.03, and 0.42 ± 0.03 ms for the control and 1 and 10 μM BCTC, respectively; $p < 0.001$). Greater changes in closed compared with open intervals are readily apparent in the one- and two-dimensional dwell-time distributions (Fig. 2, *B* and *C*, respectively), where BCTC dramatically shifted closed intervals from briefer to longer, with smaller shifts in open intervals from longer to briefer. Significant shifts at the level of the individual exponential components were limited to a decrease in the area of the faster closed component (EC1) and to increases in some of the time constants and areas of the two slowest closed com-

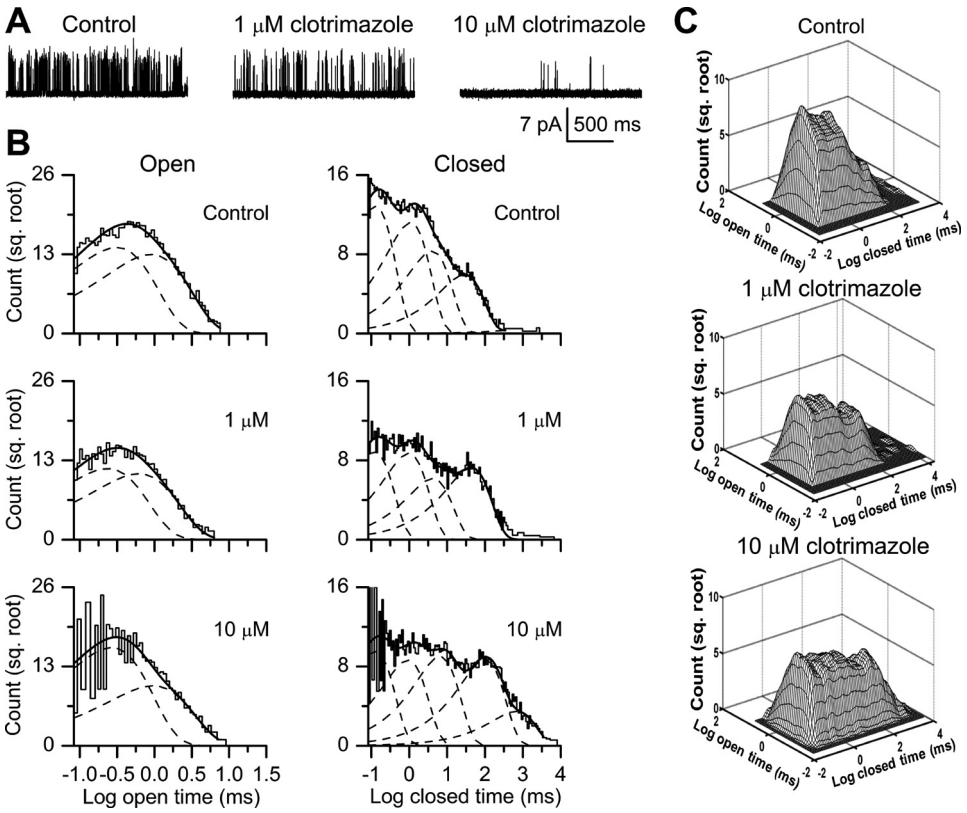

FIGURE 3. **Effects of clotrimazole on single-channel TRPM8 currents.** *A*, representative traces of single-channel activity in 0 (control), 1, and 10 μM clotrimazole recorded from the same patch at room temperature. *B*, open and closed one-dimensional dwell-time histograms. The histograms have been fitted (*continuous lines*) by the sum of two open and five closed exponential components (*dashed lines*). *sq.*, square. *C*, two-dimensional dwell-time distributions.

ponents (EC4 and EC5) with increasing BCTC concentration (supplemental Table S2).

The same types of experiments using the antifungal compound clotrimazole led to shifts in mean interval durations and distributions similar to those observed for BCTC. Increasing clotrimazole concentrations decreased TRPM8 P_o (Fig. 3*A*) from a control value of 0.12 ± 0.02 to 0.09 ± 0.04 with 1 μM clotrimazole and to 0.02 ± 0.01 with 10 μM clotrimazole ($n = 6$; $p = 0.0055$). These changes in P_o resulted from an increase in the mean closed time from 7.7 ± 2.8 to 13 ± 4 ms with 1 μM clotrimazole and to 50 ± 8 ms with 10 μM clotrimazole ($n = 6$; $p = 0.0055$) and from a decrease in the mean open time from 0.74 ± 0.02 to 0.58 ± 0.03 ms with 10 μM clotrimazole ($n = 6$; $p = 0.029$). No change was observed in mean open time between the control (0.74 ± 0.02 ms) and 1 μM clotrimazole (0.74 ± 0.10 ms). As was the case with BCTC and sM8-6 isoforms, the increase in the mean closed time was considerably greater (~7-fold between the control and 10 μM clotrimazole) than the modest decrease in the mean open time (<2-fold between the control and 10 μM clotrimazole). These shifts in closed times to longer durations with clotrimazole are readily apparent in the one- and two-dimensional dwell-time distributions (Fig. 3, *B* and *C*), with a significant decrease in the area of the fastest closed component (EC1) (supplemental Table S3) and significant increases in the time constants and/or areas of the two slowest components (EC4 and EC5) (supplemental Table S3).

Action of BCTC, Clotrimazole, and sM8-6 Isoforms on TRPM8 Channels Can Be Described by Seven-state Kinetic Model—To relate the single-channel recordings to a kinetic gating mechanism for TRPM8 channels, the two-dimensional dwell-time distributions obtained from the single-channel recordings in the absence and presence of the different modulators were individually fitted to a seven-state kinetic scheme (Fig. 4), previously shown to be consistent with WT TRPM8 gating (15), using maximum likelihood methods (see "Experimental Procedures"). The most likely rate constants for the transitions among the various states for the controls and different modulators are provided in supplemental Tables S4–S6. To examine if the seven-state kinetic model and estimated rate constants could account for the single-channel gating seen with the various modulators, the one- and two-dimensional distributions predicted by the kinetic model were compared with the experimental distributions. The predicted distributions for sM8-6 isoforms (supplemental Fig. S2), BCTC (supplemental Fig. S3), and clotrimazole (supplemental Fig. S4) can be compared with the experimental distributions in Figs. 1–3 and supplemental Fig. S1. For all three modulators, the predicted distributions gave reasonable descriptions of the experimental distributions. Thus, the general gating mechanism described by the seven-state model describes the gating of TRPM8 in the presence of sM8-6 isoforms, BCTC, and clotrimazole. It has been shown previously that the same seven-state model can also account for WT TRPM8 gating at 20 °C

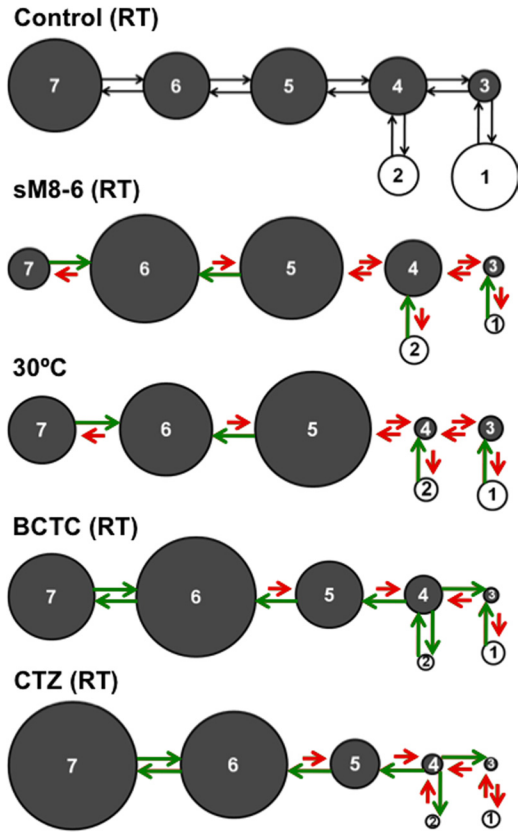

FIGURE 4. **Schematic representations of changes in rate constants and equilibrium occupancies for seven-state TRPM8 gating scheme with indicated modulators.** The *gray circles* and *open circles* are closed and open states, respectively. The areas of the circles are proportional to the equilibrium occupancies of the states. The control (*first model*) is the mean response of the separate controls for all of the experimental conditions (all obtained at room temperature), which is sufficient for visual comparisons between control and modulators. *Red arrows* indicate that a rate constant was slowed by a modulator compared with the control for that modulator, and *green arrows* indicate that a rate constant was accelerated. The rate constants for the gating under control and modulator conditions are presented in supplemental Tables S4–S6.

and when the channel is inhibited by elevating the temperature to 30 °C (15).

sM8-6 Isoforms Mimic Temperature-dependent Regulation of WT TRPM8 Channels—The observation that the seven-state model is consistent with the gating for the different modulators provides a framework within which to explore mechanisms responsible for modulation of TRPM8 channels by different agents, including temperature (15). The changes in the rate constants induced by the various modulators are schematically shown in Fig. 4. *Red arrows* indicate that the rate constant was slowed by the modulator, and *green arrows* indicate that it was accelerated. The relative equilibrium occupancies of the various states are indicated by the relative areas of the states. Whereas all of the modulators inhibited channel activity by increasing the equilibrium occupancy of the closed states at the expense of the open states, the shifts in equilibrium occupancy and the direction of change in the various rate constants could be different for different modulators, suggesting possible differences in the underlying mechanism. To explore whether there might be different mechanisms of inhibition exploited by different types of modulators, we first visually compared the shifts in the dwell-time distributions to look for similarities and differences in their action. The shift in the distributions by sM8-6 isoforms mimics, to a first approximation, the shift induced by raising the temperature from 20 to 30 °C, suggesting similarities in the underlying mechanism for sM8-6 and temperature inhibition (Fig. 1, *C* and *D*). In contrast, inhibition by BCTC or clotrimazole gave shifts in the distributions that were generally similar, but they differed considerably from the shifts induced by either sM8-6 isoforms or increased temperature (compare Figs. 1–3 and supplemental Fig. S1). These observations suggest that modulation by the two chemical inhibitors may have steps in common but differs from inhibition by sM8-6 isoforms or elevated temperature.

To test further for different classes of inhibition (H-type for heating-like inhibition and B-type for BCTC-like inhibition), the direction of the changes in each rate constant by the various modulators was examined (Fig. 4). If modulators share common mechanisms, then each modulator might be expected to move any specified rate constant in the same direction, either faster or slower (see "Experimental Procedures"). Inhibition by sM8-6 isoforms compared with a 10 °C increase in temperature moved 12 of the 12 rate constants describing the seven-state model in the same direction (Fig. 4 and supplemental Table S7). The probability of 12/12 rate constants moving in the same direction by chance alone is $p = 0.00024$ (see "Experimental Procedures," Equation 1, and supplemental Table S7). When the changes in rate constants with temperature were obtained from a previous study (corrected to +100 mV) (Tables 4 and 6 in Ref. 15), then 10 of the 12 rate constants moved in the same direction for sM8-6 inhibition compared with a 10 °C increase in temperature. The probability of 10 or more rate constants changing in the same direction by chance alone is $p = 0.0194$. These observations that sM8-6 and increased temperature moved more rate constants in the same direction than would be expected by chance alone are consistent with similarities in the underlying mechanisms of inhibition by these two modulators. Hence, sM8-6 inhibition falls into the class of H-type inhibition. Clotrimazole moved 10 of the 12 rate constants in the same direction as inhibition by BCTC ($p = 0.0194$ for 10 or more of the 12 rate constants) (Fig. 4 and supplemental Table S7), consistent with similarities in the underlying mechanism for these two chemical modulators. Hence, clotrimazole inhibition falls into the B-type class.

In contrast, when inhibition by sM8-6 or increased temperature was compared with inhibition by either clotrimazole or BCTC, only 6 ($p = 0.61$ for 6 or more) and 8 ($p = 0.19$ for 8 or more) of the 12 rate constants, respectively, moved in the same direction, consistent with chance alone (Fig. 4 and supplemental Table S7). This suggests that differences exist in the gating mechanism responsible for H-type and B-type inhibition. Hence, both the visual shifts in the dwell-time distributions and the direction of change in the rate constants suggest that sM8-6 reduces channel activity in a manner that more closely resembles inhibition by increasing temperature than inhibition by the chemical inhibitors BCTC and clotrimazole. Different inhibitors in the same class may induce similar directional changes in the rate constants by shifting the gating into a mode common

for that class, with a different mode of gating for each class of inhibitor.

Comparing shifts in rate constants induced by changing the membrane potential from +100 to 0 mV (15) to those induced by the examined inhibitors indicated that 5 of the 12 rate constants were shifted in the same direction by hyperpolarization as by BCTC, 3 of 12 for clotrimazole, 7 of 12 for sM8-6, and 7 of 12 for heating. Hence, inhibition by the examined modulators involves some major differences in mechanism compared with decreasing channel activity by hyperpolarization, as might be expected.

DISCUSSION

In this study, we used single-channel analysis to explore the kinetic mechanisms underlying the modulation of TRPM8 channels by short TRPM8 isoforms (sM8-6) and several chemical compounds. For this detailed analysis, expression of the sM8β splice variant was used because it encodes only one dominant sM8-6 protein, whereas expression of sM8α results in two proteins (10). The single-channel kinetics during modulation were found to be consistent with the previously published seven-state kinetic scheme (15). Comparison of the effects of different modulators and temperature elevation provided insights into the underlying mechanism. The kinetic mechanisms underlying inhibition by sM8-6 isoforms and elevated temperature (heating) have many features in common (H-type inhibitors), as do those responsible for inhibition by BCTC and clotrimazole (B-type inhibitors), but there are major kinetic differences between H-type and B-type inhibitors (Fig. 4 and supplemental Table S7).

Voets *et al.* (28) showed previously that mutations in S4 reduce the gating charge of TRPM8 and also alter the thermosensitivity, suggesting that voltage sensors may be associated with S4 and that there is coupling between voltage and temperature activation. The demonstration by Brauchi *et al.* (29) that switching the entire C-terminal domains between the heat receptor TRPV1 and the cold receptor TRPM8 reverses the thermosensitivity of these channels indicates that the key thermosensitive structures are contained in the cytoplasmic region of the channels. Because of the difference in location of voltage sensors and thermosensors, it might be expected that temperature and voltage coupling would be separable, and this has been shown to be the case for several thermo-TRP channels, including TRPV1, TRPV3, and TRPM8 (30–33), *e.g.* voltage-dependent but temperature-insensitive mutant TRPM8 channels have been described (30). Therefore, it might also be expected that some of the directional changes in rate constants for inhibition by hyperpolarization and heating would be different, as described under "Results." Interestingly, although somewhat weaker, the coupling between temperature stimuli and channel gating is still maintained in TRPV1/TRPM8 chimeric channels (29). Despite this molecular complexity, it is clear, however, that depolarization and cold synergize in TRPM8 activation (seen as $V_{½}$ temperature dependence and $t_{½}$ voltage dependence), and consistent with this, the single-channel gating mechanism in terms of states and connections among states of TRPM8 activation by depolarization and cold is practically identical (15). Hence, the picture emerging is that there are different classes of polymodal modulators for TRPM8, with similarities in the mechanism for modulators in the same class and differences in the mechanism for modulators in different classes. We thus propose two general types of TRPM8 inhibition in addition to hyperpolarization, H-type (heating-like) and B-type (BCTC-like), for ease of reference and kinetic action. In the context discussed above, the possibility of reduced coupling or even dissociation between voltage and temperature regulation in mutant thermo-TRP channels (29–33) serves an important caution that similar kinetic action does not establish that the underlying physical actions are identical, only that they have similar kinetic effects on the gating.

Fernández *et al.* (15) have shown previously that shifting voltage in the negative direction or increasing temperature inhibits TRPM8 channels mainly by increasing the durations of the closed intervals, similar to the effects of sM8-6 isoforms and the chemical inhibitors BCTC and clotrimazole. Thus, inhibition of TRPM8 channels by all means examined so far results mainly from an increase in the mean closed time, with fewer brief closings and increased numbers and durations of longer closings, with less effect on the open time distributions (Figs. 1–3). Major changes in closed dwell times compared with the open ones have also been detected for capsaicin-induced TRPV1 currents (34, 35), indicating some possible gating similarities between these two thermosensing channels. Similarly, TRPC4 activation by agonists and G proteins shifts gating toward pairs of the shortest closures and longest openings when P_o is largest (36).

If the inhibitors sM8-6, BCTC, and clotrimazole acted by blocking the pore, then they might be expected to reduce single-channel conductance if they are "fast" blockers or to add a closed component whose area increases proportionally to blocker concentration and with a fixed time constant equal to the blocker occupancy duration if they are "slow" blockers. Based on the data presented here and in the preceding article (10), there are no changes in single-channel conductance and no additional closed components related to possible blocked states, but changes in the relative occupancy of the different kinetic states are evident (Figs. 1–4). Hence, an allosteric mode of action, which stabilizes closed states, seems likely for TRPM8 regulation by the examined inhibitors.

We (10) have shown that the dominant-negative effect exerted by short TRPM8 isoforms on TRPM8 proteins relates to their interaction with the C terminus of WT TRPM8 ion channels. A similar conclusion using different methods was also drawn by Brauchi *et al.* (29) with regard to the effect of cold/warm temperatures on TRPM8 gating such that the TRPM8 temperature-sensing machinery is contained in the C terminus. Thus, these previous observations and our new observations of similar kinetic mechanisms underlying temperature and sM8-6 inhibition suggest that sM8-6 inhibition may be through the temperature-sensitive regulatory machinery, possibly in the C terminus. This piggyback mechanism of action of sM8-6 isoforms may explain the pervasive physiological presence of TRPM8 channels and sM8-6 isoforms in tissues where there is little temperature variation, *i.e.* the temperature machinery is exploited for inhibition by sM8-6 isoforms.

REFERENCES

1. McKemy, D. D., Neuhausser, W. M., and Julius, D. (2002) Identification of a cold receptor reveals a general role for TRP channels in thermosensation. *Nature* **416,** 52–58
2. Peier, A. M., Moqrich, A., Hergarden, A. C., Reeve, A. J., Andersson, D. A., Story, G. M., Earley, T. J., Dragoni, I., McIntyre, P., Bevan, S., and Patapoutian, A. (2002) A TRP channel that senses cold stimuli and menthol. *Cell* **108,** 705–715
3. Patel, T., Ishiuji, Y., and Yosipovitch, G. (2007) Menthol: a refreshing look at this ancient compound. *J. Am. Acad. Dermatol.* **57,** 873–878
4. Mälkiä, A., Madrid, R., Meseguer, V., de la Peña, E., Valero, M., Belmonte, C., and Viana, F. (2007) Bidirectional shifts of TRPM8 channel gating by temperature and chemical agents modulate the cold sensitivity of mammalian thermoreceptors. *J. Physiol.* **581,** 155–174
5. Behrendt, H. J., Germann, T., Gillen, C., Hatt, H., and Jostock, R. (2004) Characterization of the mouse cold-menthol receptor TRPM8 and vanilloid receptor type-1 VR1 using a fluorometric imaging plate reader (FLIPR) assay. *Br. J. Pharmacol.* **141,** 737–745
6. Weil, A., Moore, S. E., Waite, N. J., Randall, A., and Gunthorpe, M. J. (2005) Conservation of functional and pharmacological properties in the distantly related temperature sensors TRVP1 and TRPM8. *Mol. Pharmacol.* **68,** 518–527
7. Madrid, R., Donovan-Rodríguez, T., Meseguer, V., Acosta, M. C., Belmonte, C., and Viana, F. (2006) Contribution of TRPM8 channels to cold transduction in primary sensory neurons and peripheral nerve terminals. *J. Neurosci.* **26,** 12512–12525
8. Malkia, A., Pertusa, M., Fernández-Ballester, G., Ferrer-Montiel, A., and Viana, F. (2009) Differential role of the menthol-binding residue Y745 in the antagonism of thermally gated TRPM8 channels. *Mol. Pain* **5,** 62–75
9. Meseguer, V., Karashima, Y., Talavera, K., D'Hoedt, D., Donovan-Rodríguez, T., Viana, F., Nilius, B., and Voets, T. (2008) Transient receptor potential channels in sensory neurons are targets of the antimycotic agent clotrimazole. *J. Neurosci.* **28,** 576–586
10. Bidaux, G., Beck, B., Zholos, A., Gordienko, D., Lemonnier, L., Flourakis, M., Roudbaraki, M., Borowiec, A. S., Fernández, J., Delcourt, P., Lepage, G., Shuba, Y., Skryma, R., and Prevarskaya, N. (2012) *J. Biol. Chem.* **287,** 2948–2962
11. Gkika, D., and Prevarskaya, N. (2009) Molecular mechanisms of TRP regulation in tumor growth and metastasis. *Biochim. Biophys. Acta* **1793,** 953–958
12. Ramsey, I. S., Delling, M., and Clapham, D. E. (2006) An introduction to TRP channels. *Annu. Rev. Physiol.* **68,** 619–647
13. Otsuguro, K., Tang, J., Tang, Y., Xiao, R., Freichel, M., Tsvilovskyy, V., Ito, S., Flockerzi, V., Zhu, M. X., and Zholos, A. V. (2008) Isoform-specific inhibition of TRPC4 channel by phosphatidylinositol 4,5-bisphosphate. *J. Biol. Chem.* **283,** 10026–10036
14. Chu, X., Tong, Q., Wozney, J., Zhang, W., Cheung, J. Y., Conrad, K., Mazack, V., Stahl, R., Barber, D. L., and Miller, B. A. (2005) Identification of an N-terminal TRPC2 splice variant which inhibits calcium influx. *Cell Calcium* **37,** 173–182
15. Fernández, J. A., Skryma, R., Bidaux, G., Magleby, K. L., Scholfield, C. N., McGeown, J. G., Prevarskaya, N., and Zholos, A. V. (2011) Voltage- and cold-dependent gating of single TRPM8 ion channels. *J. Gen. Physiol.* **137,** 173–195
16. Vanden Abeele, F., Zholos, A., Bidaux, G., Shuba, Y., Thebault, S., Beck, B., Flourakis, M., Panchin, Y., Skryma, R., and Prevarskaya, N. (2006) Ca^{2+}-independent phospholipase A_2-dependent gating of TRPM8 by lysophospholipids. *J. Biol. Chem.* **281,** 40174–40182
17. Qin, F., Auerbach, A., and Sachs, F. (1996) Estimating single-channel kinetic parameters from idealized patch-clamp data containing missed events. *Biophys. J.* **70,** 264–280
18. Qin, F., Auerbach, A., and Sachs, F. (1997) Maximum likelihood estimation of aggregated Markov processes. *Proc. Biol. Sci.* **264,** 375–383
19. Colquhoun, D., and Sigworth, F. J. (1995) in *Single-Channel Recording* (Sakmann, B., and Neher, E., eds) pp. 483–587, Plenum Press, New York
20. Sigworth, F. J., and Sine, S. M. (1987) Data transformations for improved display and fitting of single-channel dwell time histograms. *Biophys. J.* **52,** 1047–1054
21. Horn, R., and Lange, K. (1983) Estimating kinetic constants from single channel data. *Biophys. J.* **43,** 207–223
22. Magleby, K. L., and Song, L. (1992) Dependency plots suggest the kinetic structure of ion channels. *Proc. Biol. Sci.* **249,** 133–142
23. Rothberg, B. S., Bello, R. A., and Magleby, K. L. (1997) Two-dimensional components and hidden dependencies provide insight into ion channel gating mechanisms. *Biophys. J.* **72,** 2524–2544
24. Blatz, A. L., and Magleby, K. L. (1986) Correcting single channel data for missed events. *Biophys. J.* **49,** 967–980
25. Hawkes, A. G., Jalali, A., and Colquhoun, D. (1992) Asymptotic distributions of apparent open times and shut times in a single channel record allowing for the omission of brief events. *Philos. Trans. R. Soc. Lond. B Biol. Sci.* **337,** 383–404
26. Rothberg, B. S., and Magleby, K. L. (1998) Kinetic structure of large-conductance Ca^{2+}-activated K^+ channels suggests that the gating includes transitions through intermediate or secondary states. A mechanism for flickers. *J. Gen. Physiol.* **111,** 751–780
27. Rothberg, B. S., and Magleby, K. L. (2000) Voltage and Ca^{2+} activation of single large-conductance Ca^{2+}-activated K^+ channels described by a two-tiered allosteric gating mechanism. *J. Gen. Physiol.* **116,** 75–99
28. Voets, T., Owsianik, G., Janssens, A., Talavera, K., and Nilius, B. (2007) TRPM8 voltage sensor mutants reveal a mechanism for integrating thermal and chemical stimuli. *Nat. Chem. Biol.* **3,** 174–182
29. Brauchi, S., Orta, G., Salazar, M., Rosenmann, E., and Latorre, R. (2006) A hot-sensing cold receptor: C-terminal domain determines thermosensation in transient receptor potential channels. *J. Neurosci.* **26,** 4835–4840
30. Brauchi, S., Orta, G., Mascayano, C., Salazar, M., Raddatz, N., Urbina, H., Rosenmann, E., Gonzalez-Nilo, F., and Latorre, R. (2007) Dissection of the components for PIP_2 activation and thermosensation in TRP channels. *Proc. Natl. Acad. Sci. U.S.A.* **104,** 10246–10251
31. Latorre, R., Brauchi, S., Orta, G., Zaelzer, C., and Vargas, G. (2007) ThermoTRP channels as modular proteins with allosteric gating. *Cell Calcium* **42,** 427–438
32. Grandl, J., Hu, H., Bandell, M., Bursulaya, B., Schmidt, M., Petrus, M., and Patapoutian, A. (2008) Pore region of TRPV3 ion channel is specifically required for heat activation. *Nat. Neurosci.* **11,** 1007–1013
33. Grandl, J., Kim, S. E., Uzzell, V., Bursulaya, B., Petrus, M., Bandell, M., and Patapoutian, A. (2010) Temperature-induced opening of TRPV1 ion channel is stabilized by the pore domain. *Nat. Neurosci.* **13,** 708–714
34. Hui, K., Liu, B., and Qin, F. (2003) Capsaicin activation of the pain receptor, VR1: multiple open states from both partial and full binding. *Biophys. J.* **84,** 2957–2968
35. Studer, M., and McNaughton, P. A. (2010) Modulation of single-channel properties of TRPV1 by phosphorylation. *J. Physiol.* **588,** 3743–3756
36. Zholos, A. V., Zholos, A. A., and Bolton, T. B. (2004) G-protein-gated TRP-like cationic channel activated by muscarinic receptors: effect of potential on single-channel gating. *J. Gen. Physiol.* **123,** 581–598

Short Isoforms of the Cold Receptor TRPM8 Inhibit Channel Gating by Mimicking Heat Action rather than Chemical Inhibitors

J.A. Fernández, R. Skryma, G.Bidaux, K.L. Magleby, C.N. Scholfield, J.G. McGeown, N. Prevarskaya, A.V. Zholos

SUPPLEMENTAL DATA

FIGURE LEGENDS

FIGURE S1. **The 1D dwell-time distributions for TRPM8 co-expressed with sM8-6 are described by the sums of 2 open (top) and 5 closed (bottom) exponential components.** Compare to Figs. 1 C, 2 B, and 3 B for differences with WT TRPM8 data and inhibition by BCTC and clotrimazole.

FIGURE S2. **The 7-state kinetic scheme for TRPM8 shown in Figure 4 predicts the main features of the gating of TRPM8 co-expressed with sM8-6 isoforms.** *A* and *B*, the 1D histograms are for experimental data for sM8-6 isoforms from Fig. 1 C and the continuous lines are the predicted distributions from the 7-state model in Fig. 4. *C*, the 2D dwell-time distribution predicted by the kinetic scheme captures the major features of the experimental distributions (compare to Fig. 1 D, middle). The most likely rate constants were obtained by fitting the 2D experimental dwell-time distribution and were then used to simulate 100,000 open and closed intervals which were analyzed in the same way the experimental data were analyzed to generate the predicted 1D distributions in *A* and *B* and the predicted 2D dwell-time distributions in *C*. Experimental and simulated distributions were normalized to have the same numbers of events.

FIGURE S3. **The 7-state kinetic scheme shown in Figure 4 predicts the main features of the gating in the absence and presence of BCTC.** *A*, The 1D dwell-time histograms are for experimental data from Fig. 2 B and the continuous lines are the predicted distributions for the 7-state model in Fig. 4. *B*, the predicted 2D dwell-time distributions capture the major features of the experimental distributions (compare to Fig. 2 C). The most likely rate constants and predictions were obtained as described in the legend to Fig. S2.

FIGURE S4. **The 7-state kinetic scheme shown in Figure 4 predicts the main features of the gating in the absence and presence of clotrimazole.** *A*, the 1D dwell-time histograms are for experimental data from Fig. 3 B and the continuous lines are the predicted distributions for the 7-state model in Fig. 4. *B*, the predicted 2D dwell-time distributions capture the major features of the experimental distributions (compare to Fig. 3 C). The most likely rate constants and predictions were obtained as described in the legend to Fig. S2.

TABLE S1

Effects of sM8-6 isoforms on 1D exponential components

	WT TRPM8 (RT)[a]		sM8-6 (RT)[b]		WT TRPM8 (30°C)[c]	
Exp.	τ (ms)	Area	τ (ms)	Area	τ (ms)	Area
EC1	0.23 ± 0.01	0.44 ± 0.02	0.23 ± 0.09	0.14 ± 0.02**	0.26 ± 0.02	0.20 ± 0.03**
EC2	1.13 ± 0.13	0.37 ± 0.02	1.87 ± 0.49	0.31 ± 0.04	1.11 ± 0.09	0.31 ± 0.03
EC3	4.41 ± 1.05	0.16 ± 0.02	13.4 ± 4.65	0.18 ± 0.04	15.6 ± 2.99**	0.19 ± 0.04
EC4	19.2 ± 4.12	0.025 ± 0.006	48.1 ± 7.60*	0.27 ± 0.05**	67.6 ± 17.5**	0.25 ± 0.05**
EC5	2428 ± 896	0.00035 ± 0.00008	93.2 ± 16.5**	0.10 ± 0.03**	735 ± 223*	0.072 ± 0.042**
EO1	0.87 ± 0.08	0.56 ± 0.04	0.41 ± 0.06**	0.83 ± 0.08*	0.29 ± 0.03**	0.77 ± 0.03**
EO2	2.27 ± 0.27	0.44 ± 0.04	1.22 ± 0.22*	0.17 ± 0.08*	0.77 ± 0.09**	0.23 ± 0.03**

[a and c] Means ± SEM for 2 open (EO1–EO2) and 5 closed (EC1–EC5) exponential components from 8 (RT, control, two left columns) and 13 single-channel patches (30°C, two right columns). Data from (15). These mean values should not be used to calculate P_o and mean open and mean closed time. Rather separate values would need to be calculated for each channel and then averaged.

[b] Mean values from 5 single-channel patches (RT) with co-expression of sM8-6 isoforms.

[* or **] Significance according to the Mann-Whitney test (*, $P < 0.05$; **, $P < 0.01$).

TABLE S2

Effects of BCTC on 1D exponential components

	0 μM		1 μM		10 μM	
Exp.	τ (ms)	Area	τ (ms)	Area	τ (ms)	Area
EC1	0.12 ± 0.01	0.40 ± 0.02	0.12 ± 0.01	0.33 ± 0.01*	0.14 ± 0.02	0.32 ± 0.05*
EC2	0.95 ± 0.12	0.32 ± 0.03	1.29 ± 0.20	0.31 ± 0.02	1.23 ± 0.25	0.27 ± 0.04
EC3	6.07 ± 1.00	0.23 ± 0.02	11.5 ± 3.95	0.21 ± 0.01	20.3 ± 5.83	0.19 ± 0.05
EC4	25.8 ± 5.59	0.056 ± 0.009	60.5 ± 20.6**	0.15 ± 0.02	152 ± 67**	0.19 ± 0.05
EC5	6440 ± 2334	0.0005 ± 0.0001	3819 ± 1191	0.0054 ± 0.0026**	5432 ± 3194	0.029 ± 0.017**
EO1	0.30 ± 0.02	0.47 ± 0.03	0.22 ± 0.03	0.53 ± 0.07	0.25 ± 0.03	0.73 ± 0.08
EO2	0.84 ± 0.05	0.53 ± 0.03	2.77 ± 2.23	0.47 ± 0.07	1.10 ± 0.49	0.27 ± 0.08

Means ± SEM for 2 open (EO1–EO2) and 5 closed (EC1–EC5) exponential components at RT from 10 single-channel patches with increasing concentrations of BCTC (from left to right). These mean values should not be used to calculate P_o and mean open and mean closed time. Rather separate values would need to be calculated for each channel and then averaged.

* or ** Significance according to the non-parametric ANOVA test (*, $P < 0.05$; **, $P < 0.01$).

TABLE S3

Effects of clotrimazole on 1D exponential components

	0 μM		1 μM		10 μM	
Exp.	τ (ms)	Area	τ (ms)	Area	τ (ms)	Area
EC1	0.10 ± 0.01	0.46 ± 0.01	0.11 ± 0.01	0.40 ± 0.03**	0.18 ± 0.02	0.36 ± 0.03**
EC2	0.77 ± 0.08	0.28 ± 0.02	0.73 ± 0.06*	0.27 ± 0.02	1.35 ± 0.32*	0.28 ± 0.02
EC3	4.33 ± 0.33	0.21 ± 0.01	3.87 ± 0.32	0.22 ± 0.02	13.5 ± 5.63	0.19 ± 0.02
EC4	27.6 ± 5.66	0.054 ± 0.010	34.2 ± 5.22*	0.12 ± 0.02*	139 ± 49*	0.16 ± 0.04*
EC5	7123 ± 4538	0.0005 ± 0.0001	6770 ± 2653	0.0048 ± 0.0042*	10540 ± 3863	0.0096 ± 0.0056*
EO1	0.29 ± 0.02	0.42 ± 0.05	0.31 ± 0.03	0.59 ± 0.08	0.30 ± 0.03	0.65 ± 0.06
EO2	0.90 ± 0.05	0.58 ± 0.05	0.95 ± 0.13	0.41 ± 0.08	0.84 ± 0.08	0.35 ± 0.06

Means ± SEM for 2 open (EO1–EO2) and 5 closed (EC1–EC5) exponential components at RT from 6 single-channel patches with increasing concentrations of clotrimazole (from left to right). These mean values should not be used to calculate P_o and mean open and mean closed time. Rather separate values would need to be calculated for each channel and then averaged.

* or ** Significance according to the non-parametric ANOVA test (*, $P < 0.05$; **, $P < 0.01$).

TABLE S4

Rate constants (s^{-1}) for 7-state scheme with increasing BCTC

	Control (0 μM)	1 μM	10 μM
Transition	2D	2D	2D
O1-C3	2720 ± 108	3791 ± 499	3073 ± 699
C3-O1	10192 ± 1080	9612 ± 1716	7627 ± 2313
O2-C4	5071 ± 301	8942 ± 1222	12668 ± 4399
C4-O2	535 ± 77	2512 ± 1376	4310 ± 1292
C3-C4	4916 ± 247	4852 ± 761	4435 ± 852
C4-C3	983 ± 96	981 ± 189	1265 ± 450
C4-C5	733 ± 128	1806 ± 817	2841 ± 892
C5-C4	490 ± 106	327 ± 49	398 ± 138
C5-C6	66 ± 16	116 ± 22	165 ± 36
C6-C5	89 ± 19	59 ± 10*	43 ± 15*
C6-C7	0.73 ± 0.16	0.96 ± 0.26	1.46 ± 1.10
C7-C6	0.41 ± 0.13	1.26 ± 0.75	8.42 ± 7.86

Means ± SEM for rate constants from the 7-state scheme with 2 open and 5 closed states at RT fitted separately to 10 single-channel patches and increasing concentrations of BCTC (from left to right).
* or ** Significance according to the non-parametric ANOVA test (*, $P < 0.05$; **, $P < 0.01$).

TABLE S5

Rate constants (s^{-1}) for 7-state scheme with increasing clotrimazole

	Control (0 μM)	1 μM	10 μM
Transition	2D	2D	2D
O1-C3	3263 ± 276	3385 ± 114*	1718 ± 519*
C3-O1	13673 ± 928	12824 ± 1180	8443 ± 3817
O2-C4	5769 ± 702	6173 ± 564	5138 ± 468
C4-O2	507 ± 82	574 ± 75	4943 ± 1578
C3-C4	4444 ± 251	4910 ± 421	2635 ± 685
C4-C3	955 ± 63	820 ± 37	1346 ± 366
C4-C5	770 ± 131	794 ± 54	3389 ± 876
C5-C4	462 ± 70	408 ± 52	320 ± 62
C5-C6	59 ± 15	107 ± 25	138 ± 16
C6-C5	60 ± 11	47 ± 5	32 ± 5
C6-C7	0.85 ± 0.23	0.21 ± 0.06	1.30 ± 0.90
C7-C6	0.57 ± 0.21	0.16 ± 0.06	0.71 ± 0.33

Means ± SEM for rate constants from the 7-state scheme with 2 open and 5 closed states at RT fitted separately to 6 single-channel patches and increasing concentrations of clotrimazole (from left to right).

* or ** Significance according to the non-parametric ANOVA test (*, $P < 0.05$; **, $P < 0.01$).

TABLE S6

Rate constants (s^{-1}) for 7-state scheme with sM8-6 isoforms

	WT TRPM8 (RT)[a]	sM8-6 (RT)[b]	WT TRPM8 (30°C)[c]
Transition	2D	2D	2D
O1-C3	888 ± 103	1708 ± 360	3007 ± 405**
C3-O1	4125 ± 634	1683 ± 283*	3096 ± 647
O2-C4	1874 ± 176	4955 ± 859**	6179 ± 635**
C4-O2	2679 ± 551	1816 ± 781	1400 ± 370
C3-C4	2775 ± 308	1270 ± 643	1582 ± 119**
C4-C3	1623 ± 309	183 ± 112**	490 ± 144**
C4-C5	2133 ± 601	1777 ± 1370	1168 ± 312
C5-C4	906 ± 172	356 ± 214*	237 ± 87**
C5-C6	64 ± 10	197 ± 123	99 ± 57
C6-C5	121 ± 20	59 ± 20	47 ± 13**
C6-C7	2.30 ± 0.91	1.89 ± 0.51	2.20 ± 0.67
C7-C6	3.64 ± 2.55	16 ± 3*	5.73 ± 2.34

[a or c] Means ± SEM for rate constants from 7-state scheme fitted separately to 8 (RT, control, left column) and 13 single-channel patches (30°C, right column). Data from (15).

[b] Mean values from 5 single-channel patches at RT with co-expressed sM8-6 isoforms (middle column).

[* and **] Significance according to the Mann-Whitney test (*, $P < 0.05$; **, $P < 0.01$).

TABLE S7

Number of rate constants moved in the same direction by each of the compared modulators

Modulators	Number	[a]P (cumulative)
sM8-6 vs. 30°C	12/12	0.00024
BCTC vs. CTZ	10/12	0.0194
sM8-6 vs. CTZ	6/12	0.613
sM8-6 vs. BCTC	8/12	0.194
30°C vs. CTZ	6/12	0.613
30°C vs. BCTC	8/12	0.193

[a] Probability (cumulative) of observing the indicated number or more of the rate constants (out of 12) moving in the same direction for each of the indicated modulators (see Materials and Methods). sM8-6 inhibition is most like 30°C inhibition, and BCTC inhibition is most like clotrimazole (CTZ) inhibition in terms of the directions the various modulators move the rate constants.

Figure S1

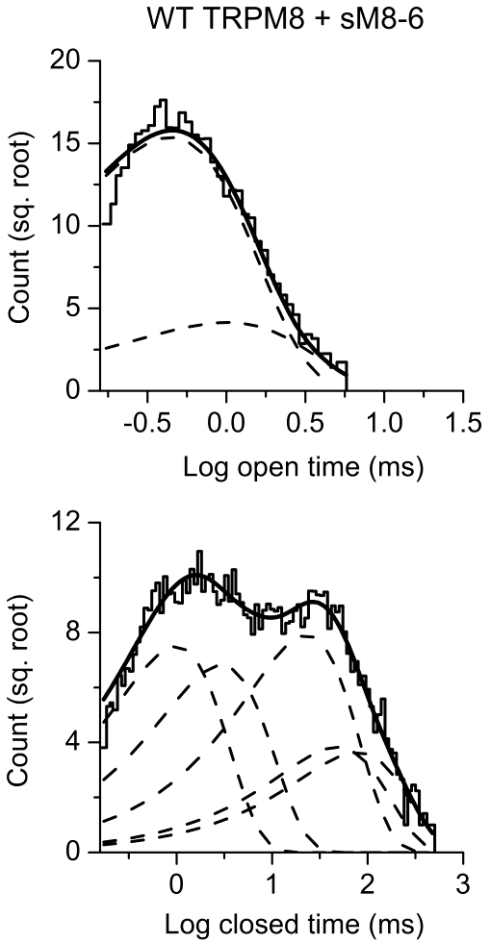

Figure S2

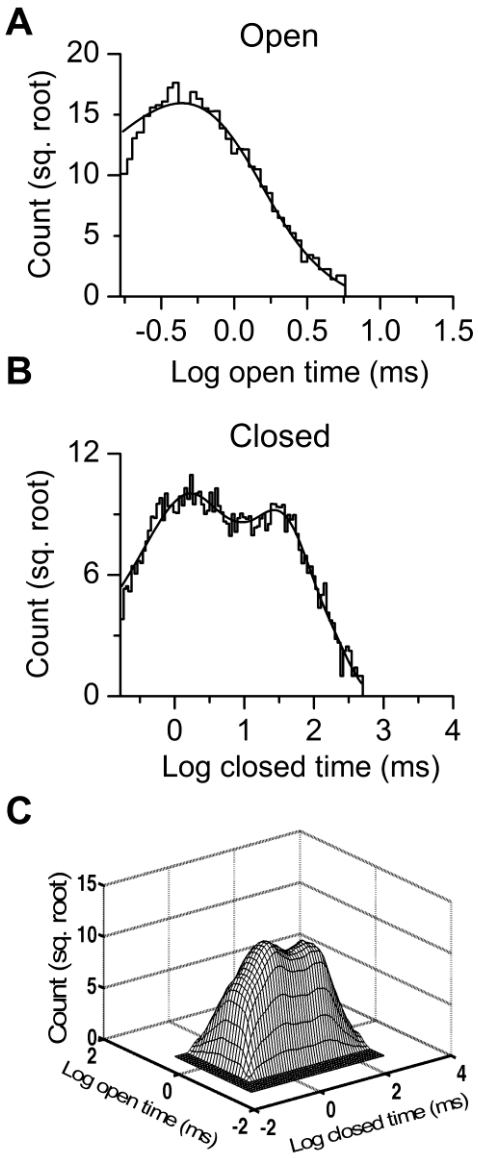

Figure S3

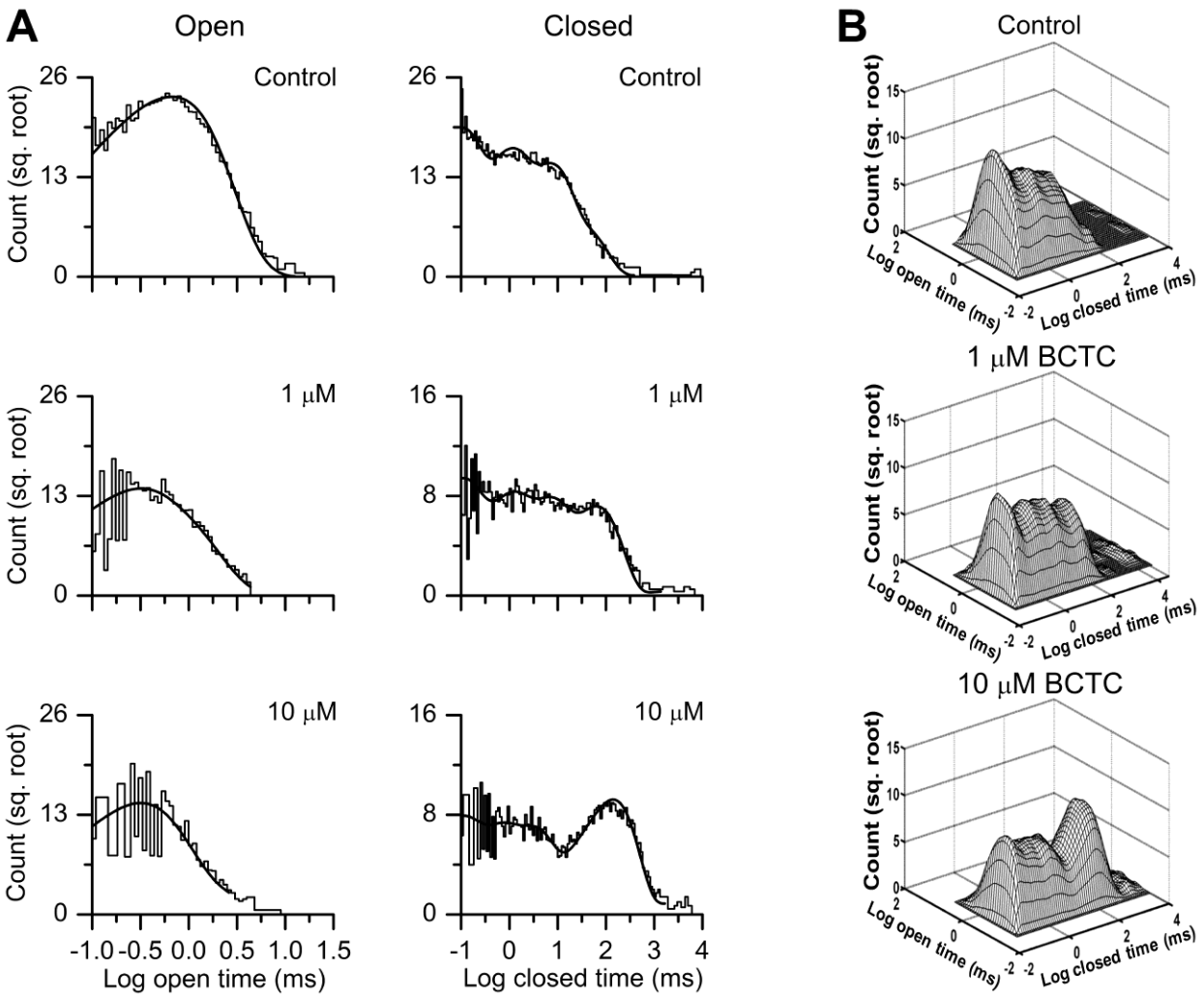

Figure S4